CHEMISTRY OF MATERIALS

Article

pubs.acs.org/cm

Origin of Abnormal Dielectric Behavior and Chemical States in Amorphous $CaCu_3Ti_4O_{12}$ Thin Films on a Flexible Polymer Substrate

Chan Su Han,[†] Hong Rak Choi,[†] Hong Je Choi, and Yong Soo Cho*

Department of Materials Science and Engineering, Yonsei University, Seoul 03722, Korea

Supporting Information

ABSTRACT: High dielectric constant thin films processable at nearly room temperature have been demanded for various flexible electronic devices. Here, we explore the origin of abnormal dielectric behavior of amorphous $CaCu_3Ti_4O_{12}$ (CCTO) thin films having an exceptionally high dielectric constant, in conjunction with chemical states and unusual ferroelectricity in the amorphous state. As an optimal example, the amorphous CCTO film sputtered at room temperature under an oxygen partial pressure of 3.6 mTorr exhibits a dielectric constant of ~192 and a dielectric loss of <0.1 at 100 Hz. The promising dielectric characteristics are unexpectedly found to originate from the evolution of ferroelectric domains, even in the amorphous state. Strong dependence of oxygen partial pressure on chemical states, vacancy formation, and ferroelectric polarization is very critical for the unexpected dielectric behavior. This may be the very first example of exploring the origin of amorphous dielectric behavior for a material that possesses space charge polarization.

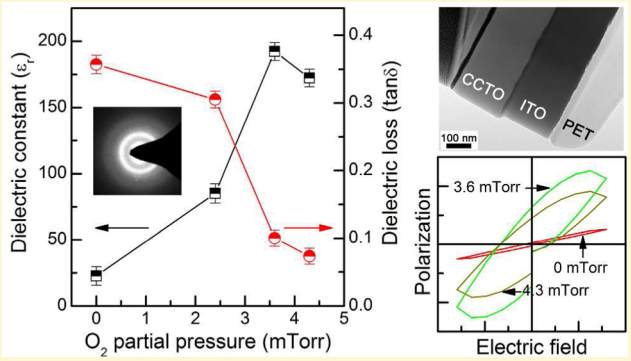

INTRODUCTION

High dielectric constant ε_r thin films have been studied to realize better device performance in various passive and active components. These devices require high capacitance mainly for storing more charges and/or for reducing the operating voltage.[1−5] In the past decade, there has been increased interest in accommodating high ε_r thin films, particularly for flexible electronic systems that require low-temperature processing compatible with most polymer-based substrates. The direct deposition of high ε_r thin films on polymer substrates is the ideal case since it does not necessitate the expensive and size-limited transfer process of separately prepared thin films. Most of the high ε_r thin films remain as amorphous state at the polymer-compatible processing temperatures even though the crystallinity of the films depends on the type of material and deposition method.[6,7] Therefore, there have always been limitations in realizing competitive performance in the flexible electronic devices incorporating capacitive thin films. The reported amorphous high ε_r thin films, including $BaTiO_3$,[8] $Pb(Zr,Ti)O_3$,[9] Y_2CuTiO_6,[10] $ZrTiO_4$,[11] HfO_2,[12] $HfLaO_x$,[13] and $YScO_3$,[14] exhibit dielectric constants typically in the range of ~10 to ~130, which originates from ionic or dipolar (orientational) polarization. Interestingly, there have been very limited reports dealing with high ε_r thin films deposited on flexible polymer substrates.[15,16] Most of the studies on the amorphous dielectric thin films were conducted on the basis of a rigid substrate like Si.

On the other hand, body-centered cubic perovskite $CaCu_3Ti_4O_{12}$ (CCTO) has unique advantages of a giant dielectric constant (>10^4) as well as minimal temperature dependence of ε_r between 100 and 600 K.[17,18] Numerous efforts have been undertaken to understand the properties of crystalline $CaCu_3Ti_4O_{12}$ and to explore the origin of the unusually high ε_r in the form of bulk and crystalline thin films.[17−22] An internal barrier layer capacitor (IBLC) model based on n-type semiconducting grains and insulating grain boundaries in polycrystalline CCTO is known to be responsible for the giant dielectric permittivity.[20−22] The structural complexity is associated with the defect chemistry and the mixed chemical states of cations. For example, the n-type conductivity of grains is known to come from the potential reduction of Ti^{4+} to Ti^{3+}, which occurs as the electrons released from oxygen vacancies are accepted by the conduction band of Ti^{4+}.[23] A potential barrier at the grain boundary inhibits the electronic transport and induces a larger polarization with accumulated charges. The interfacial polarization mechanism by larger dipoles across the grain boundaries is understood as the main contributor to the giant ε_r, which is very rare since many other perovskite ferroelectrics do not possess the intrinsic nature of interfacial polarization. Typically, interfacial polarization is induced in ferroelectric $BaTiO_3$ for a giant dielectric constant by post-heat-treating in a reducing atmosphere to control the chemical states of grain boundaries.[24,25] From this point of view, studies on amorphous CCTO

Received: April 1, 2017
Revised: June 30, 2017
Published: July 5, 2017

DOI: 10.1021/acs.chemmater.7b01346
Chem. Mater. 2017, 29, 5915−5921

thin films would be very interesting since grain boundaries do not exist in the amorphous state.

This work introduces amorphous high ε_r thin films of $CaCu_3Ti_4O_{12}$ (CCTO) sputter-deposited at room temperature, which possess ε_r close to 200 with reasonably low loss tangent and good transparency of >80% at visible wavelengths. The dielectric properties of amorphous CCTO thin films have not been reported so far. As a main parameter, oxygen partial pressure is varied to control the chemical states of the films and thus to modulate their dielectric properties. Unexpected ferroelectricity is assumed to be responsible for the unusually high ε_r in spite of the amorphous state. The ferroelectric state was recently reported to exist in the bulk CCTO ceramics, which originates potentially from the electronic density modulations and the physical displacement of Ti ions in the TiO_6 octahedra.[26,27] Here, the origin of such abnormal dielectric behavior in the amorphous state is explored in conjunction with the potential polarization mechanism on the basis of supporting evidence for the changed chemical states and domain formation

EXPERIMENTAL SECTION

Preparation of Amorphous CCTO Thin Films. $CaCu_3Ti_4O_{12}$ thin films were grown at room temperature on indium thin oxide (ITO: ~210 nm thick)-coated polyethylene terephthalate (PET) substrates by rf magnetron sputtering using a 2 in. stoichiometric CCTO target. The target was prepared by the conventional solid state reaction of $CaCO_3$ (99.5%, Showa Chemicals, Tokyo, Japan), CuO (99.0%, High Purity Chemicals, Tokyo, Japan), and TiO_2 (99.8%, Ferro Co., Cleveland, OH) at 1000 °C, followed by hot-pressing at 1100 °C under a pressure of 15 MPa in a N_2 atmosphere. The substrates were tilted by ~30° with respect to the target normal.[28] The distance between the centers of target and substrate was kept at 7 cm. The sputtering chamber was evacuated to a base pressure of 5×10^{-6} Torr using a turbomolecular pump backed by a rotary pump. A constant working pressure of 7.2 mTorr was maintained by adjusting the throttle valve while allowing different argon−oxygen gas mixtures through a mass-flow controller. The different gas mixtures are expressed in terms of the oxygen partial pressure from 0 to 4.3 mTorr. For example, an oxygen partial pressure of 4.3 mTorr was obtained by using an Ar/O_2 ratio of 30/45 in sccm. Prior to the deposition, presputtering was carried out for 10 min. The film with a thickness of ~300 nm was obtained as a result of rf magnetron sputtering with a constant rf power of 100 W at 13.56 MHz at room temperature for 90 min. The substrate holder was rotated at 8 rotations per min about its axis during the deposition.

Characterization. Crystal structures of the thin films were examined using an X-ray diffractometer (XRD: Ultima IV, Rigaku) with Cu−Kα radiation in Bragg-Bretano ($\theta/2\theta$) geometry in range of 2θ = 20−80°. Cross-sectional transmission electron microscopy (TEM) specimens were prepared using a standard focused ion beam (FIB) technique. The detailed microstructural investigations were performed using high-resolution TEM (HRTEM; Tecnai G2 F30 S-Twin, FEI) equipped with a high-angle annular dark-field (HAADF) detector. High-resolution X-ray photoelectron spectroscopy (Escalab 220i-XL, VG Scientific Instrument) using Al Kα photons (1486.6 eV) was carried out at a base pressure of ~1.1×10^{-10} Torr in an ultra-high-vacuum (UHV) chamber after Ar etching of the sample. The shifts of the core-level spectra were corrected by calibration with the C 1s peak at 285 eV. The thickness of the films was determined by direct observation of the cross-sectional image obtained by field emission scanning electron microscopy (FESEM: S-4700, Hitachi). The films were further characterized by piezoresponse force microscopy (PFM: Nanoscope V multimode, Bruker) at a resonant frequency of 330 kHz, and typically, at a force constant of 42 N m^{-1} using a Pt/Ir-coated Si cantilever. Piezoelectric response amplitude over the local surface area of the films was measured using PFM incorporating a lock-in technique with an applied AC voltage (driving amplitude: 4000 mV). Optical transmittance of the films was measured by a UV−visible spectrophotometer (V-530, JASCO). A metal−insulator−metal sandwich structure on which a Pt top electrode of ~250 nm was deposited by DC sputtering was fabricated, and the dielectric properties were evaluated at room temperature by an impedance analyzer (4294A, Agilent). Ferroelectric hysteresis loops and leakage currents were measured by using an RT66A ferroelectric test system (236, Keithley) and an electrometer (6517A, Keithley), respectively.

RESULTS AND DISCUSSION

Figure 1a shows the XRD patterns of the thin films deposited at different oxygen partial pressures from 0 to 4.3 mTorr. For

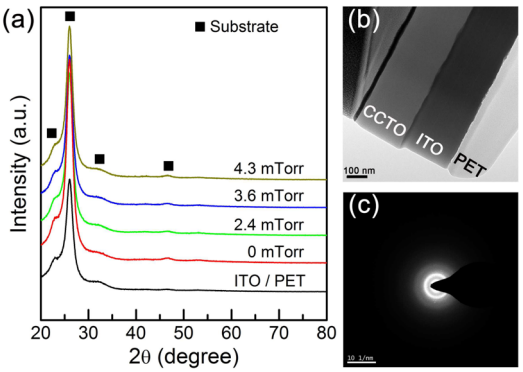

Figure 1. (a) XRD patterns of CCTO thin films sputter-deposited at different oxygen partial pressures, (b) a cross-sectional TEM image representing individual CCTO and ITO layers on a PET substrate, and (c) a condensed diffraction pattern of the CCTO thin film deposited at the oxygen partial pressure of 4.3 mTorr, indicating the amorphous state of the films.

comparison, the XRD pattern of the ITO/PET substrate is included. It is clearly seen that the deposition at room temperature does not induce crystallization, regardless of the oxygen partial pressure. An example of a cross-sectional TEM for the 4.3 mTorr sample is illustrated in Figure 1b, which reveals the clear interface between the dielectric layer and the ITO electrode. The condensed diffraction pattern in Figure 1c confirms the amorphous nature of the CCTO film. Additional TEM results for the 0 mTorr sample can be referred to Figure S1 of the Supporting Information. We also confirmed the amorphous state from the Raman spectra of the CCTO films as shown in Figure S2, where the symmetry peaks associated with the rotation/vibration of TiO_6 octahedra are not present at any level of oxygen partial pressure. It should be mentioned that the films are kept highly transparent regardless of oxygen pressure, as seen in the transmittance curves of Figure S3.

High-resolution XPS spectra of the Cu 2p and Ti 2p regions for the CCTO thin films deposited at different oxygen partial pressures were investigated to confirm the variations in the chemical states. All XPS results are shown in Figure S4. Figure 2 presents examples of the XPS spectra for the films deposited at 4.3 mTorr, with the variations in the charge valence ratios of Cu^{2+}/Cu^{1+} and Ti^{4+}/Ti^{3+} with increasing oxygen flow. The binding energy values were calibrated using the C 1s peak at 285 eV as an internal standard. The XPS spectra in Figure 2a include two peaks at ~932 and ~941 eV, which originate from the binding energy of the Cu $2p_{3/2}$ states. The curves were fitted by using Lorentzian−Gaussian functions and Shirley backgrounds. The fitted curves suggest the coexistence of the $Cu^{1+}$and Cu^{2+} valence states. The Cu^{2+}/Cu^{1+} ratio was

DOI: 10.1021/acs.chemmater.7b01346
Chem. Mater. 2017, 29, 5915−5921

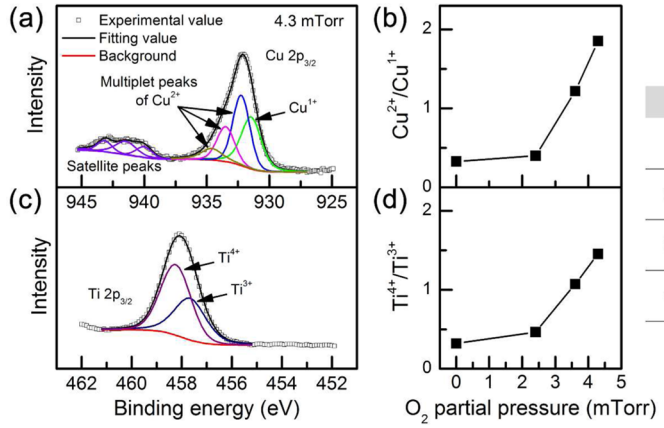

		Ca	Cu	Ti	O
0 mTorr	at. %	5.1	15.0	20.4	59.5
	Ratio	1	2.98	4.04	11.8
2.4 mTorr	at. %	5.0	15.0	20.2	59.8
	Ratio	1	2.99	4.04	11.94
3.6 mTorr	at. %	5.0	15.0	20.1	59.9
	Ratio	1	3.01	4.02	11.98
4.3 mTorr	at. %	5.0	15.1	20.0	60.0
	Ratio	1	3.02	4.01	12.03

Figure 2. (a, c) High-resolution XPS spectra of the Cu 2p and Ti 2p regions for the CCTO thin films deposited at 4.3 mTorr and the variations in the valence ratios of (b) Cu^{2+}/Cu^{1+} and (d) Ti^{4+}/Ti^{3+} as a function of oxygen partial pressure. The inserted table represents the atomic concentration in percentage and the ratio of Ca:Cu:Ti:O for the samples processed with different oxygen partial pressures.

calculated from the peak areas to trace the changes in the Cu valence state as a function of oxygen flow, as shown in Figure 2b. The Cu^{2+}/Cu^{1+} ratio increased gradually from 0.33 to 1.89 as the oxygen partial pressure increased. The gradual transition into the Cu^{2+} state is believed to be associated with the sacrificing of oxygen vacancies with the incremental supply of oxygen, as expected by the simple reaction $V_o^{\bullet\bullet} + O^{2-} = O_o$.[29] Oxygen vacancies were reported to exist in crystalline CCTO films prepared by rf sputtering under low oxygen pressures.[30] The decrease in the number of oxygen vacancies might contribute largely to minimizing the charge imbalance toward the stoichiometric CCTO structure in the amorphous structure and, thus, to influencing chemical states of cations.[31,32]

As another example, Figure 2c also shows the Ti $2p_{3/2}$ states of the XPS spectra for the films deposited at 4.3 mTorr pressure. The spectra could be divided into the contributions from Ti^{3+} and Ti^{4+} as a result of the identical curve fitting. The Ti^{4+}/Ti^{3+} ratios were also estimated from the peak areas for the samples processed at different oxygen partial pressures, as shown in Figure 2d. A gradual increase in the Ti^{4+}/Ti^{3+} ratio was observed with increasing oxygen flow. The gradual dominance of Ti^{4+} is similarly assumed to result from the expected oxidation of Ti^{3+} during rf sputtering, with the increased oxygen supply.

In addition, the atomic concentration and the ratio of Ca:Cu:Ti:O are presented in the inserted table of Figure 2. The values were estimated from the relative area of each element's curve in the XPS spectra according to different oxygen partial pressures as reported elsewhere.[32] The result suggests that the increase of oxygen partial pressure approaches the stoichiometric ratio (Ca:Cu:Ti:O = 1:3:4:12) of CCTO even in the amorphous state, particularly with the gradual increase of oxygen concentration.

Figure 3a shows the plots of leakage current density J versus electric field E for the amorphous CCTO thin films deposited under various oxygen flows. At a given electric field, the leakage current density considerably decreased upon increasing the oxygen flow. In addition, the breakdown voltage increased from 207 to 430 kV/cm upon increasing the oxygen partial pressure up to 4.3 mTorr. There is no reported value of leakage current for amorphous CCTO thin films, but crystalline CCTO films are reported to show a leakage current of 1250 kV/cm.[33] It is about one-third of the crystalline value, which is still meaningful

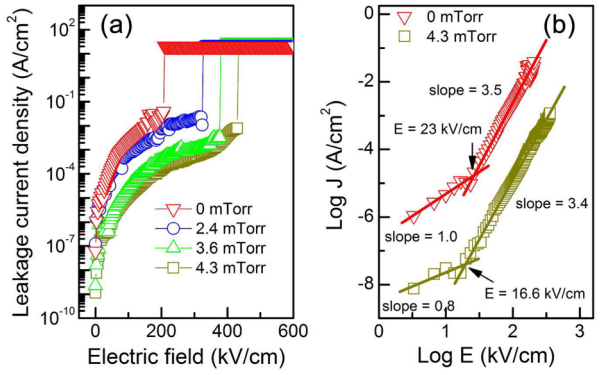

Figure 3. (a) Leakage current density (J) versus electric field (E) curves of the CCTO thin films deposited at various oxygen partial pressures, and (b) the corresponding (log J)−(log E) plots of the CCTO thin films deposited at 0 and 4.3 mTorr oxygen partial pressures, as examples.

compared to the typical leakage currents (200−500 kV/cm) for amorphous high ε_r thin films.[34,35]

The leakage current was further investigated by examining the slopes of the log J versus log E plots, as shown in Figure 3b. Regardless of the oxygen partial pressure, both curves demonstrate two distinguishable regions depending on the slope change with the electric field. At low bias fields, the slopes are close to 1, indicating the Ohmic conduction behavior, which is typically observed at low voltage or high temperature, where current is dominantly carried by the bulk-generated carriers in dielectric thin films, and not by the injected carriers from the electrodes.[36−38] At high electric fields, both the curves exhibit larger slopes of ∼3.5, indicating a change in the conduction mechanism from Ohmic conduction to Schottky emission, where the injected carriers are dominant, as reported for other amorphous dielectric thin films.[39] The film grown in the absence of oxygen flow exhibits a change in the conduction mechanism at a higher field of 23 kV/cm as compared to that (16.6 kV/cm) for the film deposited at 4.3 mTorr. The late transition at 0 mTorr may be associated with the presence of oxygen vacancies.[37,40] Oxygen vacancies contribute to the creation of additional free carriers for the bulk conduction of films. This observation agrees well with previous reports that demonstrated different conduction mechanisms in $BiFeO_3$ films depending on the density of oxygen vacancies.[40,41]

DOI: 10.1021/acs.chemmater.7b01346
Chem. Mater. 2017, 29, 5915−5921

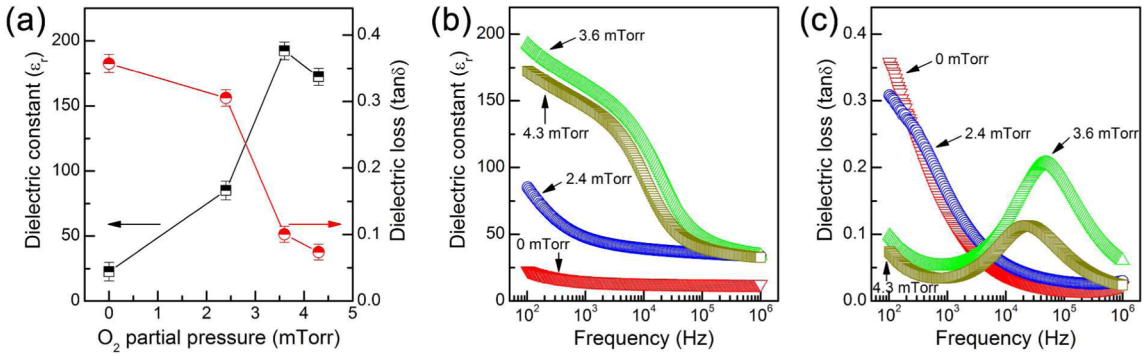

Figure 4. (a) Dielectric constant and dielectric loss of the CCTO thin films as a function of oxygen partial pressure, which were measured at 100 Hz, and the frequency dependence of (b) dielectric constant and (c) dielectric loss of the CCTO thin films deposited at different oxygen partial pressures in the frequency range of ~10^2 to 10^6 Hz, demonstrating dielectric relaxation and resonance behaviors.

Figure 4a shows the oxygen partial pressure dependence of the dielectric permittivity and dielectric loss of the amorphous CCTO thin films at 100 Hz. The dielectric properties depended on the level of oxygen flow. With an increase in oxygen flow, the dielectric constant increased up to ~192 at 3.6 mTorr and then slightly decreased to ~170 at 4.3 mTorr. The origin of the unexpectedly high permittivity will be discussed later. The dielectric loss decreased from 0.357 at zero oxygen to 0.073 at 4.3 mTorr pressure. The ε_r and tan δ values are very noticeable since they can be useful for various capacitive and transistor applications specifically requiring room temperature processing. There is no dielectric value reported for amorphous CCTO films so far. Particularly, the loss value of less than 0.1 is very meaningful since most of the amorphous colossal ε_r thin films have shown higher tan δ values of >0.10.[42,43]

Figure 4b,c shows the frequency dependence (10^2 to 10^6 Hz) of the dielectric permittivity and dielectric loss of the amorphous CCTO thin films at room temperature. The dielectric behavior with frequency was strongly dependent on the oxygen partial pressure. The dielectric constant of the 3.6 and 4.3 mTorr films (Figure 4b) shows an abrupt decrease in the frequency range of ~10^4–10^5 Hz, while no such relaxation behavior is noticeable at low oxygen partial pressures of 0 and 2.4 mTorr. This observation indicates that the polarization mechanisms differ depending on the oxygen partial pressure, which determines the relative permittivity of the amorphous samples. The relaxation process observed for the 3.6 and 4.3 mTorr films is very similar to the reported frequency dependency for crystalline CCTO thin films or bulk CCTO. The distinct resonance peaks in the dielectric loss curves of the 3.6 and 4.3 mTorr films well support the dielectric relaxation behavior.

To explore the origin of the abnormal dielectric behavior, we measured the polarization–electric field (P–E) hysteresis loop curves of the amorphous CCTO thin films deposited at different oxygen partial pressures, as shown in Figure 5a. With an increase in the oxygen partial pressure, the P–E loops of the amorphous CCTO thin films exhibited characteristics typical of ferroelectric materials. In order to ensure the reliability of the ferroelectric behavior, the P–E hysteresis loops were measured at different electric fields for the amorphous CCTO thin films deposited at 0 and 4.3 mTorr, as shown in Figure 5b. With increasing applied electric field, the remnant polarization and coercive field increased, which implies that these films possess a ferroelectric nature. The distinct ferroelectric hysteresis behavior with the increased oxygen partial pressure is assumed

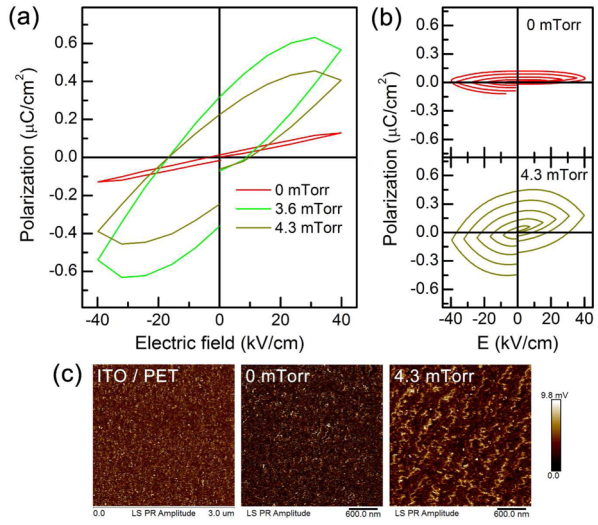

Figure 5. (a) Polarization (P)–electric field (E) hysteresis loop curves of the CCTO thin films deposited at different oxygen partial pressures, (b) cycling P–E hysteresis loops of the CCTO thin films deposited at 0 and 4.3 mTorr, and (c) the piezoresponse images of amplitude distribution over the CCTO thin films deposited at 0 and 4.3 mTorr, with the image of ITO/PET as a reference.

to be associated with the reduction in oxygen vacancy and the changed chemical states of cations.[44,45] It is known that the existence of an oxygen vacancy affects polarization negatively by acting as a clamping center against the domain wall movement.[46,47] Here, the increase in oxygen partial pressure reduces the concentration of oxygen vacancy and thus facilitates the domain movement. On the other hand, the origin of ferroelectricity itself is likely due to structural instabilities resulting from off-centered displacements of Ti ions in TiO_6 octahedra even in the amorphous state.[48] It is reported that the displacement by Ti ions is about 0.04 Å in polycrystalline CCTO ceramics and contributes to the spontaneous polarization by ~0.4 μC/cm^2.[49] In addition, the increased concentration of Ti^{4+} relative to Ti^{3+} with increasing the oxygen partial pressure is assumed to produce greater polarization because the smaller ionic size of Ti^{4+} (0.605 Å) than that of Ti^{3+}(0.67 Å) may induce a larger dipole moment.[26]

In order to further ensure the intrinsic nature of the observed ferroelectric behavior for the amorphous CCTO thin films, piezoresponse force microscopy (PFM) studies were performed, as shown in Figure 5c. The PFM image of the thin film

DOI: 10.1021/acs.chemmater.7b01346
Chem. Mater. 2017, 29, 5915–5921

deposited without oxygen flow exhibited no image contrast. However, the PFM image of the film deposited at 4.3 mTorr clearly shows a bright and dark contrast-mixed state, which was extracted by different piezoresponse amplitudes, indicating the presence of electric domains with ~10 nm scale. It is very interesting to observe the formation of domains in amorphous states from the hysteresis loops and direct amplitude images. The assumed ferroelectric behavior may also be due to the higher Ti^{4+} concentration, as observed from the XPS results for the CCTO film deposited at the oxygen partial pressure of 4.3 mTorr.

From the dielectric relaxation behavior in conjunction with the $P-E$ curves and PFM results, the samples processed at 3.6 and 4.3 mTorr seem to have the ferroelectric nature even in the amorphous state. Accordingly, the dielectric relaxation at 10^4-10^5 Hz for the 3.6 and 4.3 mTorr films (Figure 4b,c) is likely to be related to the dipolar polarization. This behavior in the amorphous state is surely abnormal since this characteristic, known as Debye-like dielectric relaxation, is generally expected for crystalline CCTO films.[20,50,51] Additionally, we assume that the low frequency rises of dielectric constant and loss at ~10^2 Hz in Figure 4b,c come from the space charge polarization at the interface between the films and electrodes.

Figure 6 shows the complex impedance curves of the amorphous CCTO thin films deposited at different oxygen

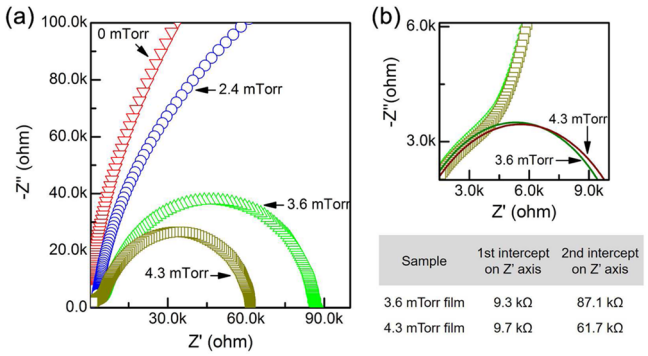

Sample	1st intercept on Z' axis	2nd intercept on Z' axis
3.6 mTorr film	9.3 kΩ	87.1 kΩ
4.3 mTorr film	9.7 kΩ	61.7 kΩ

Figure 6. (a) Complex impedance curves of the CCTO thin films deposited at different oxygen partial pressures and (b) highlighted low impedance regions of the 3.6 and 4.3 mTorr samples. The inserted table presents the real resistance values as the intercepts on the Z' axis.

partial pressures. The plots of the films deposited under oxygen partial pressures of 0 and 2.4 mTorr may assume a very large semicircle beyond the measurable frequency as shown in Figure 6a. However, the amorphous thin films deposited above 3.6 and 4.3 mTorr exhibited clear semicircles with near zero intercepts on the Z' axis at high frequency. The intercepts correspond to the resistance at the interface between the film and electrode as reported for the other amorphous films.[52] The increased oxygen partial pressure definitely reduced the interface resistance. It may be related to less defects and chemical states in the interface regions depending on the oxygen pressure.

Interestingly, the 3.6 and 4.3 mTorr films showed additional small arcs as illustrated in Figure 6b. It is very rare to observe the two arcs in the amorphous state since the first intercept on the Z' axis may indicate the existence of grain boundary resistance. Even if we assume no existence of grain boundary since it is in the amorphous state, it is presumable that there is still a certain irregularity which is acting similarly like a grain boundary. Note that the high oxygen pressure films possessed ferroelectric domains. The first and second intercept values of the samples are represented in the inserted table of Figure 6: the second intercept values correspond to the interface resistance. The first intercept value of resistance is around 9.3–9.7 kΩ, which is interestingly very close to the 9.3 kΩ value reported as a grain boundary resistance for polycrystalline $CaCu_3Ti_4O_{12}$ thin films.[22] Accordingly, domain boundary or short-range grain boundary may explain the unusual observation of resistance contributor. All the facts point out the unexpected existence of ferroelectricity and thus dipolar polarization, which must be the origin of the high dielectric constant.

In addition, we conducted extra experiments by annealing the deposited CCTO thin films up to 850 °C to verify whether the as-deposited films create a pure crystalline CCTO phase or not. For the crystalline state of CCTO thin films, the phase development and basic properties, ε_r, P_s, and effective piezoelectric coefficient, $d_{33,eff}$, can be referred to Figures S5 and S6, respectively, in the Supporting Information. Table S1 compares particularly the reported ε_r values for the cases of thin films prepared with different processing conditions.

CONCLUSIONS

We report the unusually high dielectric constant of amorphous CCTO thin films, which is very interesting since the CCTO material is known to possess space-charge polarization driven by a high resistance grain boundary in the crystalline state. As an optimal example, a dielectric constant of ~192, with a reasonably low dielectric loss < 0.1, is obtained for amorphous CCTO thin films sputter-deposited at room temperature. Dielectric properties are strongly dependent on oxygen partial pressure, as the chemical states of ions close to stoichiometric CCTO exhibit the optimal dielectric characteristics. Strong evidence of ferroelectricity even in the amorphous state, as confirmed by a hysteresis loop and domain formation, is regarded as the origin of the high dielectric constant at the specific oxygen pressure. Dielectric relaxation behavior and complex impedance analysis further support the potential dipolar polarization along with the interfacial polarization of film/electrode. The excellent dielectric characteristics are extensively applicable for flexible passive and active electronic devices requiring high dielectric constant and near room temperature processing.

ASSOCIATED CONTENT

Supporting Information

The Supporting Information is available free of charge on the ACS Publications website at DOI: 10.1021/acs.chemmater.7b01346.

Additional TEM images, Raman spectra, transmittance curves, XPS curves, XRD patterns, PFM images, and performance comparison chart in full scale (PDF)

AUTHOR INFORMATION

Corresponding Author

*E-mail: ycho@yonsei.ac.kr.

ORCID

Yong Soo Cho: 0000-0002-1601-6395

Author Contributions

†C.S.H. and H.R.C. contributed equally to this work.

DOI: 10.1021/acs.chemmater.7b01346
Chem. Mater. 2017, 29, 5915–5921

Notes

The authors declare no competing financial interest.

■ ACKNOWLEDGMENTS

This work was financially supported by a grant (NRF-2016M3A7B4910151) of the National Research Foundation of Korea.

■ REFERENCES

(1) Kingon, A. I.; Maria, J. P.; Streiffer, S. K. Alternative Dielectrics to Silicon Dioxide for Memory and Logic Devices. *Nature* **2000**, *406*, 1032−1038.
(2) Robertson, J. High Dielectric Constant Oxides. *Eur. Phys. J.: Appl. Phys.* **2004**, *28*, 265−291.
(3) Wang, T.; Ekerdt, J. G. Structure versus Thermal Stability: The Periodic Structure of Atomic Layer Deposition-Grown Al-Incorporated HfO2 Films and Its Effects on Amorphous Stabilization. *Chem. Mater.* **2011**, *23*, 1679−1685.
(4) Yang, K.; Huang, X.; Huang, Y.; Xie, L.; Jiang, P. Fluoro-Polymer@$BaTiO_3$ Hybrid Nanoparticles Prepared via RAFT Polymerization: Toward Ferroelectric Polymer Nanocomposites with High Dielectric Constant and Low Dielectric Loss for Energy Storage Application. *Chem. Mater.* **2013**, *25*, 2327−2338.
(5) Hou, R. Z.; Wu, A.; Vilarinho, P. M. Low-Temperature Hydrothermal Deposition of $(Ba_xSr_{1-x})TiO_3$ Thin Films on Flexible Polymeric Substrates for Embedded Applications. *Chem. Mater.* **2009**, *21*, 1214−1220.
(6) Kim, H.; McIntyre, P. C.; Saraswat, K. C. Effects of crystallization on the electrical properties of ultrathin dielectrics grown by atomic layer deposition. *Appl. Phys. Lett.* **2003**, *82*, 106−108.
(7) Cho, Y. J.; Nguyen, N. V.; Richter, C. A.; Ehrstein, J. R.; Lee, B. H.; Lee, J. C. Spectroscopic ellipsometry characterization of high-k dielectric HfO_2 thin films and the high-temperature annealing effects on their optical properties. *Appl. Phys. Lett.* **2002**, *80*, 1249−1251.
(8) Sreenivas, K.; Mansingh, A.; Sayer, M. Structural and electrical properties of rf-sputtered amorphous barium titanate thin films. *J. Appl. Phys.* **1987**, *62*, 4475−4481.
(9) Deng, J.; Zhu, W.; Tan, O. K.; Yao, X. Amorphous $Pb(Zr,Ti)O_3$ thin film hydrogen gas sensor. *Sens. Actuators, B* **2001**, *77*, 416−420.
(10) Monteduro, A. G.; Ameer, Z.; Martino, M.; Caricato, A. P.; Tasco, V.; Lekshmi, I. C.; Rinaldi, R.; Hazarika, A.; Choudhury, D.; Sarma, D. D.; Maruccio, G. Dielectric investigation of high-k yttrium copper titanate thin films. *J. Mater. Chem. C* **2016**, *4*, 1080−1087.
(11) Zhao, X.; Wang, S.; Li, A.; Ouyang, J.; Xia, G.; Zhou, J. Universal solution-processed high-k amorphous oxide dielectrics for high-performance organic thin film transistors. *RSC Adv.* **2014**, *4*, 14890−14895.
(12) Li, F. M.; Bayer, B. C.; Hofmann, S.; Dutson, J. D.; Wakeham, S. J.; Thwaites, M. J.; Milne, W. I.; Flewitt, A. J. High-k (k = 30) amorphous hafnium oxide films from high rate room temperature deposition. *Appl. Phys. Lett.* **2011**, *98*, 252903.
(13) Ko, J.; Kim, J.; Park, S. Y.; Lee, E.; Kim, K.; Lim, K. H.; Kim, Y. S. Solution-processed amorphous hafnium-lanthanum oxide gate insulator for oxide thin-film transistors. *J. Mater. Chem. C* **2014**, *2*, 1050−1056.
(14) Lu, C.; Lee, C. H.; Nishimura, T.; Toriumi, A. Yttrium scandate thin film as alternative high-permittivity dielectric for germanium gate stack formation. *Appl. Phys. Lett.* **2015**, *107*, 072904.
(15) Mo, Z.; Wu, G.; Bao, D. Room-temperature preparation and dielectric properties of amorphous $Bi_{3.95}Er_{0.05}Ti_3O_{12}$ thin films on flexible polyimide substrates via pulsed laser deposition method. *Appl. Surf. Sci.* **2012**, *258*, 5323−5327.
(16) Meena, J. S.; Chu, M.; Tiwari, J. N.; You, H.; Wu, C.; Ko, F. Flexible metal-insulator-metal capacitor using plasma enhanced binary hafnium-zirconium-oxide as gate dielectric layer. *Microelectron. Reliab.* **2010**, *50*, 652−656.
(17) Zhang, L. Electrode and Grain-Boundary Effects on the Conductivity of $CaCu_3Ti_4O_{12}$. *Appl. Phys. Lett.* **2005**, *87*, 022907.
(18) Homes, C. C.; Vogt, T.; Shapiro, S. M.; Wakimoto, S.; Ramirez, A. P. Optical Response of High-Dielectric-Constant Perovskite-Related Oxide. *Science* **2001**, *293*, 673−676.
(19) Deng, G.; Yamada, T.; Muralt, P. Evidence for the Existence of a Metal-Insulator-Semiconductor Junction at the Electrode Interfaces of $CaCu_3Ti_4O_{12}$ Thin Film Capacitors. *Appl. Phys. Lett.* **2007**, *91*, 202903.
(20) Sinclair, D. C.; Adams, T. B.; Morrison, F. D.; West, A. R. $CaCu_3Ti_4O_{12}$ One-Step Internal Barrier Layer Capacitor. *Appl. Phys. Lett.* **2002**, *80*, 2153−2155.
(21) Kim, B. K.; Lee, H. S.; Lee, J. W.; Lee, S. E.; Cho, Y. S. Dielectric and Grain-Boundary Characteristics of Hot Pressed $CaCu_3Ti_4O_{12}$. *J. Am. Ceram. Soc.* **2010**, *93*, 2419−2422.
(22) Kang, H. M.; Baek, S. H.; Song, J. H.; Cho, Y. S.; Choi, J. W. Full Range Dielectric Characteristics of Calcium Copper Titanate Thin Films Prepared by Continuous Composition-Spread Sputtering. *ACS Comb. Sci.* **2014**, *16*, 478−484.
(23) Zhang, L.; Tang, Z. J. Polaron Relaxation and Variable-Range-Hopping Conductivity in The Giant-Dielectric-Constant Material $CaCu_3Ti_4O_{12}$. *Phys. Rev. B: Condens. Matter Mater. Phys.* **2004**, *70*, 174306.
(24) Guillemet-Fritsch, S.; Valdez-Nava, Z.; Tenailleau, C.; Lebey, T.; Durand, B.; Chane-Ching, J. Y. Colossal Permittivity in Ultrafine Grain Size $BaTiO_{3-x}$ and $Ba_{0.95}La_{0.05}TiO_{3-x}$ Materials. *Adv. Mater.* **2008**, *20*, 551−555.
(25) Song, Z.; Zhang, S.; Liu, H.; Hao, H.; Cao, M.; Li, Q.; Wang, Q.; Yao, Z.; Wang, Z.; Lanagan, M. T. Improved Energy Storage Properties Accompanied by Enhanced Interface Polarization in Annealed Microwave-Sintered BST. *J. Am. Ceram. Soc.* **2015**, *98*, 3212−3222.
(26) Prakash, B. S.; Varma, K. B. R. Ferroelectriclike and pyroelectric behavior of $CaCu_3Ti_4O_{12}$ ceramics. *Appl. Phys. Lett.* **2007**, *90*, 082903.
(27) Ke, S.; Huang, H.; Fan, H. Relaxor behavior in $CaCu_3Ti_4O_{12}$ ceramics. *Appl. Phys. Lett.* **2006**, *89*, 182904.
(28) Mohanty, B. C.; Yeon, D. H.; Kim, B. K.; Cho, Y. S. Spatial Variation in Structural, Morphological and Optical Properties of Aluminum-Doped ZnO Thin Films Grwon by 30°-Incident Radio Frequency Magnetron Sputtering. *J. Electrochem. Soc.* **2011**, *158*, P30−P35.
(29) Lim, K.; Park, J.; Ramsier, R. D.; Kim, D. G.; Kang, J. W.; Kang, Y. C. Tailoring Phase and Oxidation States of Cu by Varying Oxygen Gas Flow Rates in RF Sputter Deposition for Photovoltaic Devices. *Appl. Surf. Sci.* **2012**, *258*, 4097−4099.
(30) Lin, S. Y.; Chen, Y. C.; Wang, C. M.; Kao, K. S.; Chan, C. Y. Effect of Rapid Thermal Annealing on Sputtered $CaCu_3Ti_4O_{12}$ Thin Films. *J. Electron. Mater.* **2009**, *38*, 453−459.
(31) Liu, Y.; Kim, H.; Wang, J. J.; Li, H.; Gordon, R. G. Effects of Low Temperature O_2 Treatment on the Electrical Properties of Amorphous $LaAlO_3$ Films Made by Atomic Layer Deposition. *ECS Trans.* **2008**, *16*, 471−478.
(32) Foschini, C. R.; Tararam, R.; Simões, A. Z.; Rocha, L. S.; Santos, C. O. P.; Longo, E.; Varela, J. A. Rietveld analysis of $CaCu_3Ti_4O_{12}$ thin films obtained by RF-sputtering. *J. Mater. Sci.: Mater. Electron.* **2016**, *27*, 2175−2182.
(33) Xiao, M.; Wang, K.; Chenyang, X.; Xie, S. Nonlinear Current-Voltage Behavior of $CaCu_3Ti_4O_{12}$ Thin Films Derived from Sol-Gel Method. *J. Mater. Sci.: Mater. Electron.* **2014**, *25*, 2710−2715.
(34) Park, J. H.; Yoo, Y. B.; Lee, K. H.; Jang, W. S.; Oh, J. Y.; Chae, S. S.; Lee, H. W.; Han, S. W.; Baik, H. K. Boron-Doped Peroxo-Zirconium Oxide Dielectric for High-Performance, Low-Temperature, Solution-Processed Indium Oxide Thin-Film Transistor. *ACS Appl. Mater. Interfaces* **2013**, *5*, 8067−8075.
(35) Kim, D. H.; Cho, N. G.; Kim, H. G.; Kim, H. S.; Hong, J. M.; Kim, I. D. Low Voltage Operating $InGaZnO_4$ Thin Film Transistors Using High-k MgO-$Ba_{0.6}Sr_{0.4}TiO_3$ Composite Gate Dielectric on Plastic Substrate. *Appl. Phys. Lett.* **2008**, *93*, 032901.
(36) Lambert, M. A.; Mark, P. *Current Injection in Solids*; Academic Press: New York, NY, 1970.
(37) Chiu, F. C. A Review on Conduction Mechanisms in Dielectric Films. *Adv. Mater. Sci. Eng.* **2014**, *2014*, 578168.

DOI: 10.1021/acs.chemmater.7b01346
Chem. Mater. 2017, 29, 5915−5921

(38) Peng, C. J.; Krupanidhi, S. B. Structures and Electrical Properties of Barium Strontium Titanate Thin Films Grown by Multi-Ion-Beam Reactive Sputtering Technique. *J. Mater. Res.* **1995**, *10*, 708−726.
(39) Lee, Y.-H.; Kim, Y.-S.; Kim, D.-H.; Ju, B.-K.; Oh, M.-H. Conduction Mechanisms in Barium Tantalates Films and Modification of Interfacial Barrier Height. *IEEE Trans. Electron Devices* **2000**, *47*, 71−76.
(40) Qi, Z.; Dho, J.; Tomov, R.; blamire, M. G.; MacManus-Driscoll, J. L. Greatly Reduced Leakage Current and Conduction Mechanism in Aliovalent-Ion-Doped $BiFeO_3$. *Appl. Phys. Lett.* **2005**, *86*, 062903.
(41) Yang, H.; Wang, Y. Q.; Wang, H.; Jia, Q. X. Oxygen Concentration and Its Effect on the Leakage Current in $BiFeO_3$ Thin Films. *Appl. Phys. Lett.* **2010**, *96*, 012909.
(42) Zhu, J.; Liu, Z. G. Dielectric Properties of YSZ High-k Thin Films Fabricated at Low Temperature by Pulsed Laser Deposition. *Mater. Lett.* **2003**, *57*, 4297−4301.
(43) Gai, Z.; Cheng, Z.; Wang, X.; Zhao, L.; Yin, N.; Abah, R.; Zhao, M.; Hong, F.; Yu, Z.; Dou, S. A Colossal Dielectric Constant of an Amorphous TiO_2:(Nb, In) Film with Low Loss Fabrication at Room Temperature. *J. Mater. Chem. C* **2014**, *2*, 6790−6795.
(44) Foschini, C. R.; Tararam, R.; Simões, A. Z.; Cilense, M.; Longo, E.; Varela, J. A. $CaCu_3Ti_4O_{12}$ thin films with non-linear resistivity deposited by RF-sputtering. *J. Alloys Compd.* **2013**, *574*, 604−608.
(45) Okamura, S.; Miyata, S.; Mizutani, Y.; Nishida, T.; Shiosaki, T. Conspicuous voltage shift of D-E hysteresis loop and asymmetric depolarization in Pb-based ferroelectric thin films. *Jpn. J. Appl. Phys.* **1999**, *38*, 5364−5367.
(46) Park, C. H.; Chadi, D. J. Microscopic study of oxygen-vacancy defects in ferroelectric perovskites. *Phys. Rev. B: Condens. Matter Mater. Phys.* **1998**, *57*, R13961.
(47) Miyayama, M.; Noguchi, Y. Polarization properties and oxygen-vacancy distribution of $SrBi_2Ta_2O_9$ ceramics modified by Ce and Pr. *J. Eur. Ceram. Soc.* **2005**, *25*, 2477−2482.
(48) Tararam, R.; Bdikin, I. K.; Panwar, N.; Varela, J. A.; Bueno, P. R.; Kholkin, A. L. Nanoscale electromechanical properties of $CaCu_3Ti_4O_{12}$ ceramics. *J. Appl. Phys.* **2011**, *110*, 052019.
(49) Liu, Y.; Withers, R. L.; Wei, X. Y. Structurally frustrated relaxor ferroelectric behavior in $CaCu_3Ti_4O_{12}$. *Phys. Rev. B: Condens. Matter Mater. Phys.* **2005**, *72*, 134104.
(50) Yang, Y.; Wang, X.; Liu, B. $CaCu_3Ti_4O_{12}$ Ceramics from Different Methods: Microstructure and Dielectric. *J. Mater. Sci.: Mater. Electron.* **2014**, *25*, 146−151.
(51) Singh, L.; Kim, W. I.; Sin, B. C.; Ullah, A.; Woo, S. K.; Lee, Y. I. Study of Dielectric, AC-Impedance, Modulus Properties of 0.5 $Bi_{0.5}Na_{0.5}TiO_3$•0.5$CaCu_3Ti_4O_{12}$ Nano-Composite Synthesized by a Modified Solid State Method. *Mater. Sci. Semicond. Process.* **2015**, *31*, 386−396.
(52) Sethi, G.; Bontempo, B.; Furman, E.; Horn, M. W.; Lanagan, M. T.; Bharadwaja, S. S. N.; Li, J. Impedance Analysis of Amorphous and Polycrystalline Tantalum Oxide Sputtered Films. *J. Mater. Res.* **2011**, *26*, 745−753.

DOI: 10.1021/acs.chemmater.7b01346
Chem. Mater. 2017, 29, 5915−5921